2020

Investigating Heterogeneous Nucleation of Barite using Hydrothermal Atomic Force Microscopy and Optical Microscopy

Ankita B. Gurav
Wright State University

INVESTIGATING HETEROGENEOUS NUCLEATION OF BARITE USING HYDROTHERMAL ATOMIC FORCE MICROSCOPY AND OPTICAL MICROSCOPY

A Thesis submitted in partial fulfillment of the
requirements for the degree of
Master of Science

by

ANKITA B. GURAV

B.S., University of Mumbai, 2017

2020

Wright State University

WRIGHT STATE UNIVERSITY

GRADUATE SCHOOL

December 11, 2020

I HEREBY RECOMMEND THAT THE THESIS PREPARED UNDER MY SUPERVISION BY Ankita B. Gurav ENTITLED Investigating Heterogeneous Nucleation of Barite Using Hydrothermal Atomic Force Microscopy and Optical Microscopy BE ACCEPTED IN PARTIAL FULFILLMENT OF THE REQUIREMENTS FOR THE DEGREE OF Master of Science.

_____

Steven Higgins, Ph.D.
Department of Chemistry
College of Science and Mathematics

_____

Audrey McGowin, Ph.D., Chair
Department of Chemistry
College of Science and Mathematics

Committee on Final Examination:

_____

Steven Higgins, Ph.D.

_____

Ioana Pavel, Ph.D.

_____

David Dolson, Ph.D.

_____

Barry Milligan, Ph.D.
Interim Dean of the Graduate School

ABSTRACT

Gurav, Ankita B. M.S, Department of Chemistry, Wright State University, 2020. Investigating Heterogenous Nucleation of Barite Using Hydrothermal Atomic Force Microscopy and Optical Microscopy

In order to develop a better understanding heterogeneous nucleation of barite, barite precipitation was studied under varying experimental parameters. Hydrothermal atomic force microscopy (HAFM) and optical microscopy were used to investigate the effect of change in temperature, supersaturation and varying ratios of ions on heterogeneous nucleation of barite. In the experiments conducted at higher temperatures, the particles thus nucleated were found to display characteristic hexagonal and rhomboidal shapes. In comparing results of particle densities among different ion ratios, there is evidence suggesting that barium to sulfate ratio plays a role of promoter. Wherein, the ratios with higher [Ba^{2+}] concentration were found to show more nucleation occurring. Although, the HAFM cell was used for experimentation, optical microscopy turned out to be a more effective method for analysis of samples.

TABLE OF CONTENTS

I. INTRODUCTION……1

II. METHODS AND MATERIALS……6

A. SOLUTION PREPARATION……6

B. SAMPLE PREPARATION……6

C. NOTE ON PIRANHA SOLUTIONS……7

D. EXPERIMENTAL METHODS……8

a. PRE-MIXED SOLUTION INJECTION METHOD……8

b. IN-LINE SOLUTION MIXING METHOD……10

III. RESULTS……13

A. PRE-MIXED SOLUTION INJECTION METHOD RESULTS……13

B. IN-LINE SOLUTION MIXING METHOD RESULTS……16

IV. DISCUSSION……27

V. CONCLUSION……32

REFERENCES……33

APPENDIX A……36

APPENDIX B……37

LIST OF FIGURES

Figure 1: Schematic diagram of experimental setup showing flow path for gas (G) and fluid (W) lines in the HAFM……8

Figure 2: Revised schematic diagram of experimental setup showing flow path for gas (G) and fluid (W) lines in the HAFM……10

Figure 3: In-situ HAFM topographical images. All images are 10µm x 10µm in size with the specific experimental conditions mentioned……15

Figure 4: Figure 4: Comparison between images obtained from HAFM and optical microscope for Sample 1 of new method. (a) 10 µm Topographical HAFM scan showing lack of growth; (b) Optical microscopy image showing presence of particles……16

Figure 5: Optical microscopy images showing growth occurring in SI 2.47 solution. (a) 2x magnification image; (b) 10x magnification image showing particles ranging ~17µm x 12µm in size……18

Figure 6. Optical microscopy images showing growth occurring in SI 2.6 solution. (a) 2x magnification image; (b) 10x magnification image showing particles ranging ~8µm x 4µm in size……18

Figure 7. Optical microscopy images showing growth occurring in SI 2.7 solution. (a) 2x magnification image; (b) 10x magnification image showing particles ranging ~11µm x 8µm in size……18

Figure 8. *Particle density distribution counting images for varying SI experiment results. (Left) Image for SI 2.6. (Right) Image for SI 2.7*……19

Figure 9. Optical microscopy images showing growth occurring in SI 2.47 solution. (a) 2x magnification image; (b) 10x magnification image showing particles ranging ~5µm x 4µm in size……20

Figure 10. Optical microscopy images showing growth occurring in SI 2.47 solution. (a) 2x magnification image; (b) 10x magnification image showing particles ranging ~27µm x 20µm in size……20

Figure 11. Optical microscopy images showing growth occurring in SI 2.47 solution with a $[Ba^{2+}]$:$[SO_4^{2-}]$ ratio of 10:1. (a) 2x magnification image; (b) 10x magnification image showing particles ranging ~2µm x 2µm in size……21

LIST OF FIGURES

Figure 12. Optical microscopy images showing growth occurring in SI 2.47 solution with a $[Ba^{2+}]$:$[SO_4^{2-}]$ ratio of 1:10. (a) 2x magnification image; (b) 10x magnification image showing particles ~1µm x 1µm in size……22

Figure 13. Optical microscopy images showing growth occurring in SI 2.47 solution with a $[Ba^{2+}]$:$[SO_4^{2-}]$ ratio of 100:1. (a) 2x magnification image; (b) 10x magnification image showing particles ~10µm x 9µm in size. ……22

Figure 14. Optical microscopy images showing growth occurring in SI 2.47 solution with a $[Ba^{2+}]$:$[SO_4^{2-}]$ ratio of 1:100. (a) 2x magnification image; (b) 10x magnification image particles ~1µm x 1µm in size ……23

Figure 15. Optical microscopy images showing growth occurring in SI 2.6 solution with a $[Ba^{2+}]$:$[SO_4^{2-}]$ ratio of 10:1. (a) 2x magnification image; (b) 10x magnification image showing particles ~6µm x 4µm in size. ……24

Figure 16. Optical microscopy images showing growth occurring in SI 2.6 solution with a $[Ba^{2+}]$:$[SO_4^{2-}]$ ratio of 1:10. (a) 2x magnification image; (b) 10x magnification image showing particles ~1.4µm x 1µm in size. ……24

Figure 17. Optical microscopy images showing growth occurring in SI 2.6 solution with a $[Ba^{2+}]$:$[SO_4^{2-}]$ ratio of 100:1. (a) 2x magnification image; (b) 10x magnification image showing particles ~5µm x 4µm in size……25

Figure 18. Optical microscopy images showing growth occurring in SI 2.6 solution with a $[Ba^{2+}]$:$[SO_4^{2-}]$ ratio of 1:100. (a) 2x magnification image; (b) 10x magnification image showing particles ~5µm x 3µm in size……25

LIST OF TABLES

Table 1. Pre-mixed solution injection method experimental conditions…….....9

Table 2. In-line solution mixing method experimental conditions……12

Table 3. Particle distribution data for experimental set of SI 2.47, 2.6 and 2.7……19

I. INTRODUCTION

Formation of mineral scale due to sparingly soluble salt precipitation is a common problem plaguing many industrial processes dealing with water or other fluid systems[1] .Barite ($BaSO_4$) scale formation is of much concern as it represents one of the most problematic minerals. Precipitated barite scales are hard and adhere well to surfaces leading to increase in operating costs for industrial processes owing to difficulty of removal[2, 3]. These concerns put emphasis on the need to study the mechanisms and pathways of barite nucleation for facilitating better designing of systems to prevent such scale formation.

Barium sulfate precipitation begins with nucleation (i.e., formation of a crystalline or amorphous nucleus) followed by growth (attachment of Ba^{2+} and SO_4^{2-} ions at various sites on pre-existing particles). Nucleation can be defined as the process of emergence of a new phase from an existing higher free energy old phase[4, 5] . Nucleation proceeds with formation of a nascent nucleus of new phase present in the old phase wherein the old phase then achieves a metastable status (i.e., the transformation occurs only after passage over a free energy (FE) barrier) [6]. When considering the FE of a newly precipitated phase, one realizes that only the FE of the bulk is less than that of the solvated phase as the molecules at the surface increase the FE of the new phase. This difference between the free energies of the molecules in the bulk and those at the surface is called the interfacial free energy. It is a predominantly positive term responsible for destabilization of the nucleus. An increase or a drop in FE of the system determines whether a nucleus will grow or dissolve back into the phase. After a certain intermediate size is attained, the free energy of the system drops irrespective of growth or dissolution. This intermediate size, called the critical size, arises as a result of the Gibbs-

Thomson effect. Critical size is found to be contingent upon supersaturation in that, at higher supersaturation the FE barrier vanishes, destabilizing the old phase leading to a possibility of new phase formation by making an infinitesimally small change in any parameter. This is known as the spinodal decomposition step and the barrier between metastability and instability is known as a spinodal line[7, 8].

Critical size was found to be affected by the thermodynamics of the solution. This realisation brought on the development of the idea that nucleation could be controlled by controlling the critical size which in turn is dependent on the interfacial energy. As a result, manipulation of solution composition or supersaturation could manipulate the occurrence of nucleation[4].

Nucleation, when occurring in bulk of a system wherein the nascent nuclei is spherical in shape is known as homogeneous nucleation whereas when it occurs at a foreign surface where the nascent nuclei has the shape of a hemisphere, is known as heterogeneous nucleation. Supersaturation of a solution will eventually result in crystallization regardless of the critical size and presence of a foreign surface. In this case, the probability of nucleus formation at any given time is a function of the critical size meaning that the interfacial energy also determines the kinetics of nucleation[4]. That being said, nucleation could further proceed along the classical pathway or along a much less explored non-classical pathway.

The Classical Nucleation Theory (CNT) as it is known today was derived from application of J.W.Gibbs' ideas of thermodynamics of fluid phase nucleation to that of nucleation of solid crystals from solutions.[10]

CNT has been used to qualitatively comprehend nucleation although it falls short in making quantitative predictions. This is owing to the assumptions being made in its applications and

oversimplification of theories. CNT assumes that the driving force for nucleation is derived from the bulk of nuclei; its structure similar to that of the bulk solution phase. However, it does not give enough consideration to impedance of growth due to generation of interfacial tension and instead just makes assumptions for the same. These rather debatable assumptions are known as capillary assumptions. As mentioned earlier, the interfacial free energy being positive hinders formation of pre-critical nuclei; formation of which can only be explained as a result of randomly distributed fluctuations on microscopic scale[10]. CNT thus considers growth occurring via addition of units (i.e., atoms, ions, molecules). As opposed to CNT, non-classical nucleation pathway suggests growth and nucleation via cluster aggregation of pre-critical nuclei. Thus, the change in dynamics of pre-nucleation clusters is considered to be the driving force behind nucleation. The claims of species thus nucleated being off-equilibrium are refuted on account of thermodynamic reversibility of observed ion binding meaning they follow thermodynamics of single phase systems eliminating the presence of a phase interface[10].

In their previous studies, Ruiz-Agudo et al successfully identified an intermediate phase in barite nucleation[15]. This phase involved the formation of a liquid precursor medium wherein growth occurred by aggregation of these precursor particles and their mesoscopic transformations. In another study they suggested of amorphous precursors and metastable stages of growth going undetected owing to their shorter lifetimes [1].

The role of ion bonding and adsorption in nucleation of barite at different phase interface systems was studied by Dai and Stack [12]. In their studies they monitored growth and heterogeneous nucleation of barite at various organic water interfaces at a constant saturation index of 1.1. They observed that glass surfaces coated with organic surfactants

exhibited more heterogeneous nucleation. They used self-assembled thin films with different terminal groups such as –COOH, -SH and mixed –COOH and –SH for this purpose. The resulting [Ba^{2+}] adsorption was found to occur in the order of mixed –SH and –COOH > –COOH > -SH. However they found that only the surfaces with –SH coatings showed heterogeneous precipitation. Surface hydrophobicity thus acting as a determining factor for prevalence of nucleation over growth. They then conducted another set of experiments with –SH coated substrates where they varied the barium to sulfate ratio in solution and observed that excess of barium adsorption affected precipitation rates thus being deemed as the rate limiting step for those cases. They compared the results of the different ratios with that of ratio = 1 and found that ratio less than 1 showed slower precipitation whereas ratios greater than 1 showed faster precipitation.

Deng and Stack [19] in their recent studies discovered homogeneous precipitation to be a growth dominated process as compared to nucleation dominated heterogeneous precipitation. They also found that homogeneous nucleation persisted in slightly supersaturated solutions and did not occur in undersaturated solutions. Comparatively, heterogeneous nucleation was prevalent in supersaturated as well as undersaturated solutions. They also found out that the organic additives facilitated formation of an enriched cationic layer further enhancing nucleation rates. They used Sr rich barite solutions for their experimentation and coated SiO_2 substrates with different organic coatings such as mixed –COOH & -SH, -COOH and -SH. They concluded that controlling the size and nucleation could be possible by controlling solution super saturation. Although their studies were carried out in a Sr-rich environment and in the presence of organic additives, it proved to be of much help in understanding nucleation processes. In that, they helped us develop a better understanding of the characteristics of

nucleation and growth when studied comparatively helping us better distinguish the resulting observed phenomena. This in turn helped us while formulating the hypothesis for our research.

While homogeneous nucleation of barite has been studied meticulously, the areas of heterogeneous nucleation study remain to be uncovered. With the existence and proof of alternative pathways for nucleation being contemplated, much work remains to be done in terms of gathering evidence suggesting the same. There is little available data in the literature about the role of various control parameters such as solution supersaturation, temperature, and effect of variance of barium to sulfate ratio on heterogeneous nucleation of barite.

In an attempt to establish a relationship between the variance of control parameters mentioned earlier and nucleation, we conducted experiments resulting in heterogeneous nucleation of barite. The experiments were devised to allow tracking precipitation of barite *in situ* in an additive free method. *In situ* hydrothermal atomic force microscopy (HAFM) experiments were designed and conducted, the results for which were analysed using HAFM and optical microscopy.

II. MATERIALS AND METHODS

Solution Preparation

0.01 M stock solutions of barium chloride (Aldrich, 99.99%) and sodium sulfate (Aldrich, 99.99%) were prepared with deionized water (Millipore filtration system). The known K_{sp} for barite was $10^{-9.96}$ at 25 °C[18]. Various saturation indices (SI) were used over the course of experimentation, where SI can be defined by the following equation:

$$SI = \log \frac{\{Ba^{2+}\}\{SO_4^{2-}\}}{K_{sp,barite}} \quad (1)$$

Where, {*n*} represents the activity of species *n.*

Using the above equation, the required concentrations of solutions were calculated and solutions were diluted accordingly (See Appendix A).

Similar calculations were made to find the required volumes of solutions for the varying ratio experiments. (Calculations included in Appendix A)

Sample Preparation

Glass microscope slide coverslips were used as sample substrates. This was done so as to make it easier to detect nucleation given their uniform and homogeneous surface. The coverslips were cleaved into 5 mm square substrates after scoring with a diamond scribe. They were then cleaned using piranha solution. An acid piranha solution was used for the same. It is a mixture of concentrated sulfuric acid (H_2SO_4) and 30% hydrogen peroxide (H_2O_2) in a 3:1 ratio.

12 mL piranha solution was prepared and the sample substrate was submerged in it followed by rinsing with MilliQ water. Samples were stored under MilliQ water until further use.

Note on Piranha Solutions:

These solutions are known to rapidly oxidize organic compounds thus minimising the amount of impurities present at the sample surface. The mixing process is a highly exothermic reaction and involves production of peroxymonosulfuric acid, also known as Caro's acid [20]. Because of their highly reactive nature, piranha solutions react violently with organics and can cause explosions if stored in closed containers [21].

To ensure safe handling and avoiding skin contact, appropriate PPE should be worn while working with these solutions. Use of appropriate labcoat, acid resistant gloves, safety glasses with shields/ splash goggles/face shields, etc are recommended.

All processes involving handling should be conducted in a properly functioning fume hood with the sash adjusted to the recommended safety level. The container containing piranha should never be removed from the hood. The hood should be labelled with a warning sign indicating the presence of piranha solution and should be kept devoid of organics in presence of piranha.

Piranha solutions must only be prepared in Glassware or Teflon as it reacts with many plastics. The peroxide should slowly be added to sulfuric acid to avoid splashing due to rise in temperature. Mixture should be allowed to stabilize before using.

Piranha solutions should never be stored and must always be prepared fresh for each application.

For appropriate disposal, the used solution must be neutralized. For this purpose, a container is filled with 1 inch of dry sodium bicarbonate and covered with water. Piranha solution is slowly poured in small portions over it. This results in expulsion of CO_2 gas which should be allowed to escape before adding more piranha. This should be continued until all piranha is neutralized, adding more sodium bicarbonate as needed. The neutralized solution, if devoid of any regulated heavy metals can be poured down the drain[22].

Methods Used for Experimentation

Although a commercial AFM allows for *in situ* experimentation, it cannot facilitate rapid solution changes during experimentation. For this purpose, a custom designed HAFM was used. Details of the operation and experimental capabilities of the HAFM are described in Higgins et al[11]. However, a brief summary of the experiments has been included below.

Pre-mixed Solution Injection Method

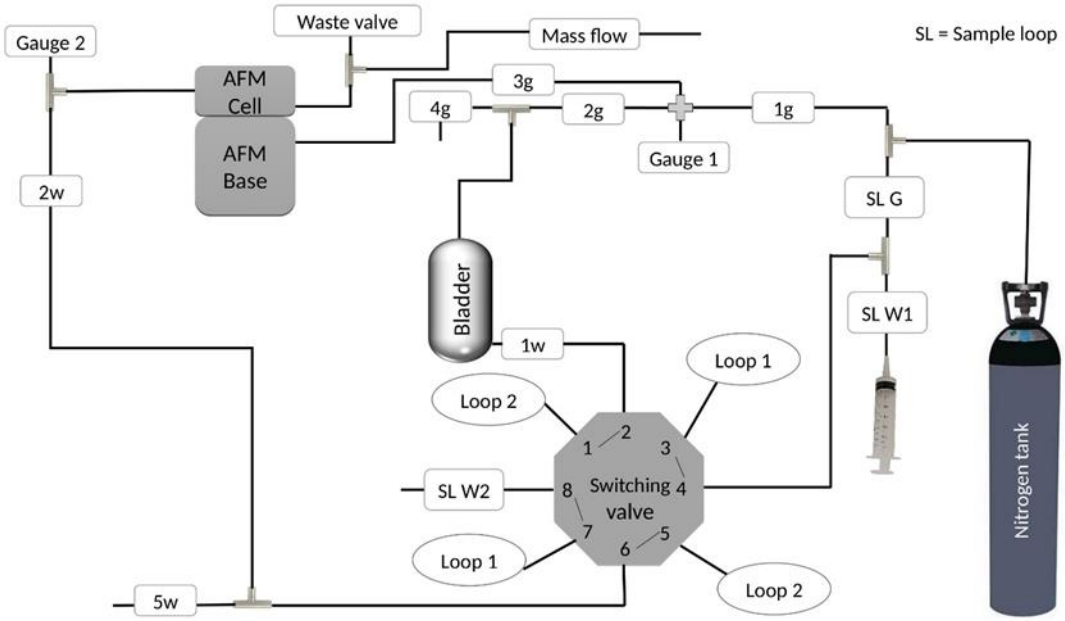

Figure 1. Schematic diagram of experimental setup showing flow path for gas (G) and fluid (W) lines in the HAFM.

A clean cleaved glass substrate was secured onto the sample mount disk in the HAFM fluid cell using a gold wire. During the setup, the sample was submerged in deionized water and kept at room temperature. The cell cover was installed and the fluid delivery system was slightly pressurized to allow for flow of water through the system. HAFM fluid cell was allowed to fill with water until it forms a small drop oozing out of the cell window space. This is done so as to eliminate presence of any air bubbles when putting on the window cover. Once the window cover is secured, system is depressurized. Once completely depressurized, the gas and water flow valves are opened at the same time to avoid formation of a pressure differential in those lines. Following this step, the system is slowly pressurized again and pressure is gradually increased to reach desired setting. At this point the flow control is turned on and set to the desired flow rate setting. Once system gets set up and stabilized, the premixed solution is injected and scanning commences. The resulting scans were analysed with PicoView software for AFM imaging and analysis by KeySight Technologies. A detailed list of experiments has been included in Table 1.

Table 1. Pre-mixed solution injection method experimental conditions

Experiment number	Attempted SI	Temperature	Pressure	Solution Flow rate	Exposure time
1	2.47	ambient	20 psi	12.5 ml/hr	5mins
				2.5 ml/hr	2 hrs 49 mins
2	2.75	ambient	20 psi	2.5 ml/hr	5 hrs 49mins
3	2.47	ambient	20 psi	2.5 ml/hr	5 hrs 50 mins
4	2.47	ambient	20 psi	12.5 ml/hr	10 mins
				2.5 ml/hr	5 hrs 32 mins
				1.25 ml/hr	4 hrs 21 mins
5	2.60	ambient	20 psi	8.75 ml/hr	1 hr 9 mins
6	2.60	ambient	20 psi	1.25 ml/hr	17 hrs 21 mins
7	2.60	40° C	20 psi	5 ml/hr	39 mins

In-line Solution Mixing Method

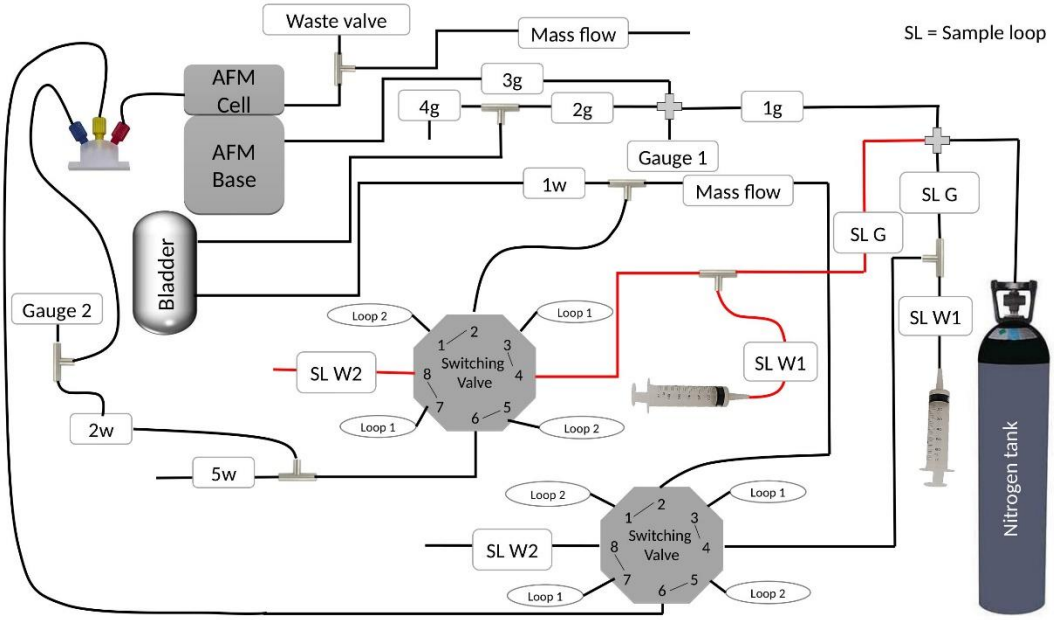

Figure 2. Revised schematic diagram of experimental setup showing flow path for gas (G) and fluid (W) lines in the HAFM

To reduce the solution delivery time to the fluid cell and counter homogeneous nucleation, the fluid delivery system was updated to include a second flow path and mixing tee. This allowed for the required solutions of $BaCl_2$ and Na_2SO_4 to be introduced separately into the system and mixed shortly before entering the fluid cell. The total flow rate for the system was set at a controlled 12.5 mL/hr. The flow rate for one loop was set at 10 mL/hr. This allowed for the flow rate of the other loop to be 2.5mL/hr as a result of the difference between the total flow rate and that of the other loops flow rate. Solutions of appropriate concentration were prepared such that the resulting mixed solution had the required saturation index (Appendix B). Details of the solutions and experimental conditions are included in Table 2. The samples thus obtained were labelled and stored in a closed sample holder to avoid

accumulation of unwanted dust particles on sample. A high power optical microscope fixed with an Infinity 2 CCD camera for capturing microscope images was utilized. Images were captured using the Infinity Analyze software allowing for camera control.

Table2. In-line solution mixing method experimental conditions

Experiment number	Attempted SI	Temperature	Pressure	Solution Flow rate $BaCl_2$	Solution Flow rate Na_2SO_4	Barium : Sulfate Ratio	Exposure time
1	2.60	ambient	20 psi	2.5 ml/hr	10 ml/hr	4:1	3 hrs 27 mins
2	2.47	ambient	20 psi	2.5 ml/hr	10 ml/hr	4:1	5 hrs 42 mins
3	2.60	ambient	20psi	2.5 ml/hr	10 ml/hr	4:1	≈2 hrs
4	2.70	ambient	20 psi	2.5 ml/hr	10 ml/hr	4:1	≈2 hrs
5	2.47	60°C	20 psi	2.5 ml/hr	10 ml/hr	4:1	≈2 hrs
6	2.47	90°C	60 psi	2.5 ml/hr	10 ml/hr	4:1	≈2 hrs
7	2.47	ambient	30 psi	2.0 ml/hr	10.5 ml/hr	10:1	2 hrs 6 mins
8	2.47	ambient	30 psi	2.0 ml/hr	10.5 ml/hr	1:10	2 hrs 3 mins
9	2.47	ambient	30 psi	2.0 ml/hr	10.5 ml/hr	100:1	2 hrs 9 mins
10	2.47	ambient	30 psi	2.0 ml/hr	10.5 ml/hr	1:100	2 hrs 4 mins
11	2.60	ambient	30 psi	2.0 ml/hr	10.5 ml/hr	10:1	2 hrs 2 mins
12	2.60	ambient	30 psi	2.0 ml/hr	10.5 ml/hr	1:10	2 hrs 1 min
13	2.60	ambient	30 psi	2.0 ml/hr	10.5 ml/hr	100:1	1 hr 58 mins
14	2.60	ambient	30 psi	2.0 ml/hr	10.5 ml/hr	1:100	2 hrs

III. RESULTS

By conducting experiments under varied temperatures and supersaturated solutions we attempted to gather evidence of heterogeneous nucleation and critical nuclei formation in barite. Owing to their metastable states, it becomes challenging to isolate and capture an amorphous phase as they can quickly transform into crystalline state[16]. Generally, stabilizing agents and additives are used to increase the lifetime of these intermediate precursors. As the role and extent of effects of these additives in the crystallization systems remains unclear, we have attempted an additive free method to investigate barite heterogeneous nucleation[1].

Results from pre-mixed solution injection method

Figure 3 shows images collected from nucleation experiments where each sample was exposed to a supersaturated solution of barium sulfate. Figure 3(a) represents control image scanned under MilliQ water. Figure 3(b) represents a topographical HAFM scan for the sample exposed to an SI 2.47 solution for an exposure time of ~3 hours. The image is a clear scan without any indication of nucleation. To better our chances of seeing nucleation, the next sample was subjected to a supersaturated solution of SI 2.75 for ~6 hours. The scanned topography for this sample is given in Figure 3(c). As in the case of its preceding sample, this sample does not show any signs of nucleation occurring. In this sample the scans started getting increasingly noisy after the initial scan collection. Repeat runs of the first experiment were conducted to confirm the lack of evidence for nucleation. In these experiments, the samples were subjected to a supersaturation of 2.47 for ~6 hours for sample 3 and ~10 hrs for sample 4. The flow rates for all the above experiments was set to 2.5 ml/hr with the exception of sample 4 where the flow rate was changed to 1.25 ml/hr after close to 6 hours. Scans for

these experiments are represented by Figure 3(d) and Figure 3(e) respectively. To further our investigation, we changed the solution supersaturation to 2.6, reduced the exposure time to an hour and increased the flow rate to 8.75 ml/hr for our next sample. Despite the changes made in experimental conditions, no growth was observed as evident from Figure 3(f). Next, we decided upon keeping the same supersaturation but changing the flow rate to 1.25 ml/hr and exposing the sample overnight (a little over 17 hrs). Topographical scan for this sample is presented as Figure 3(g). The image is devoid of particles indicative of nucleation, except for the presence of what appears to be a part of a larger particle. For our last attempt before devising another experimental method, we changed the experimental conditions, in that, we kept the supersaturation constant at 2.6 but changed the flow rate to 5 ml/hr increasing the temperature at which the experiment was conducted at 40°C. This was a comparatively shorter exposure run (~40 mins). The topographical scan for this run [Figure 3(h)] did not show any evidence of nucleation. The particles visible on the scan for this experiment were found to be present since the beginning of the experiment.

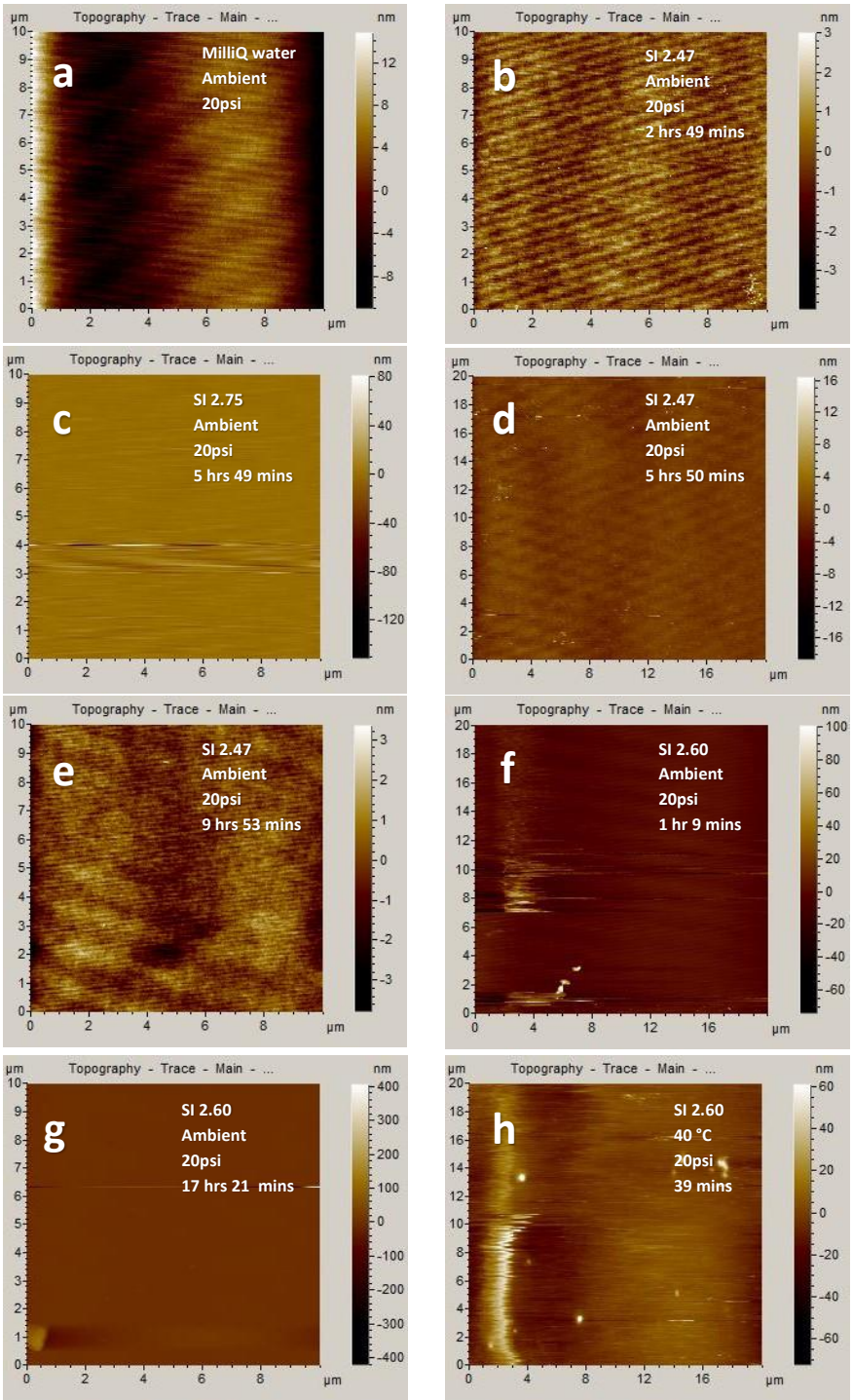

Figure 3. In-situ HAFM topographical images. All images are 10µm x 10µm in size with the specific experimental conditions mentioned.

Results from In-line solution mixing method

With no success detecting nucleation from our previous method, we devised a new method which allowed mixing of $BaCl_2$ and Na_2SO_4 solutions to attain the necessary supersaturation for the resulting $BaSO_4$ solution shortly before entering the HAFM fluid cell. This reduced the possibility of homogeneous nucleation in solution before the fluid entered the cell. The flow rates for the respective solutions were set such that the resulting flow rate for $BaSO_4$ solution was 12.5 ml/hr.

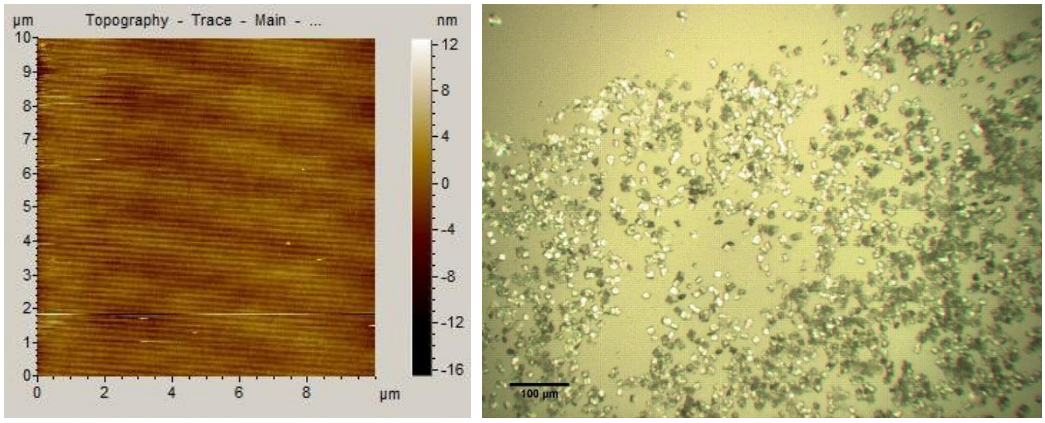

Figure 4. Comparison between images obtained from HAFM and optical microscope for Sample 1 of new method. (a) 10 µm Topographical HAFM scan showing lack of growth; (b) Optical microscopy image showing presence of particles.

The above figure displays results obtained from HAFM scan and optical microscopy wherein it is seen that although the HAFM scan is devoid of indication suggesting nucleation, optical microscopy confirms that nucleation and growth has indeed occurred. The exposure time for this sample was 3 hrs 27 mins. Supersaturation of the solution was 2.6 at ambient temperature.

As optical microscopy image provided evidence of nucleation and growth, we decided to continue analysis of our samples using an optical microscope as opposed to the HAFM. The particle sizes measured were averaged for ease of understanding.

Figure 5 shows images for an exposure time of 5 hrs 42 mins to SI 2.47 solution at ambient temperature. The particles were found to be somewhat evenly distributed and with little difference in their sizes. The particles were spaced better as compared to our previous SI 2.60 experiment as seen in Figure 4(b). The particles were mostly rectangular and square in shape.

To investigate effect of supersaturation on nucleation, a shorter exposure experiment (~2 hrs) with a solution supersaturation of 2.6 was conducted. Figure 6 shows that resulting particle size was approximately 8 µm x 4 µm.

To develop a data set for comparison purpose, another experiment was conducted under similar conditions with a solution supersaturation of 2.7 and the resulting image (Figure 7) consisted of particles approximately 11 µm x 8 µm in size.

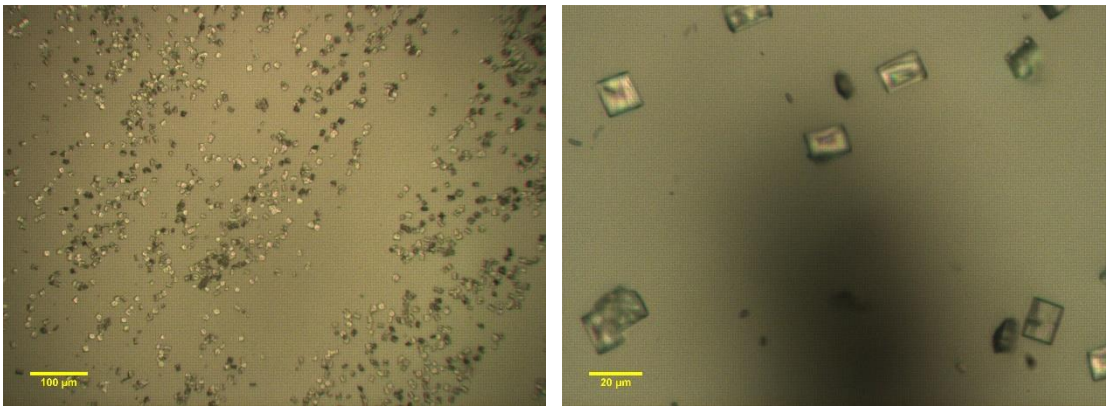

Figure 5. Optical microscopy images showing growth occurring in SI 2.47 solution at ambient temperature with exposure time of 5 hrs. 42 mins. (a) 2x magnification image; (b) 10x magnification image showing particles ~17µm x 12µm in size.

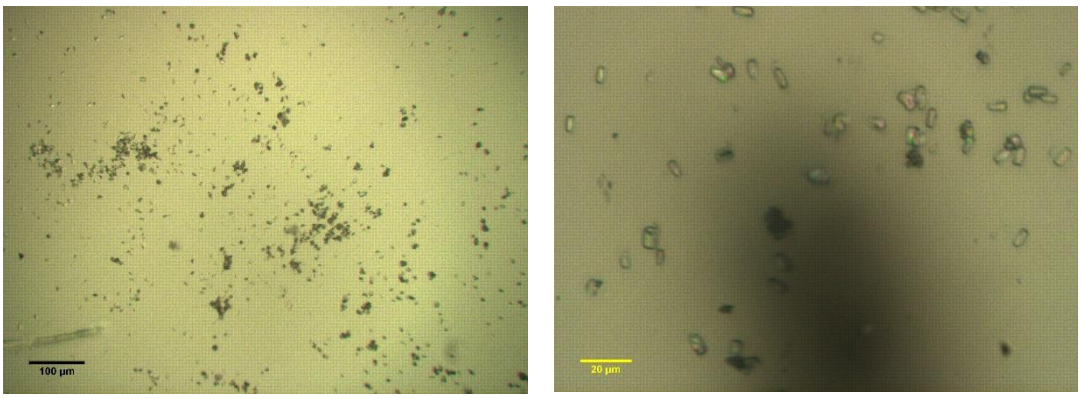

Figure 6. Optical microscopy images showing growth occurring in SI 2.6 solution at ambient temperature with exposure time of ~2 hrs. (a) 2x magnification image; (b) 10x magnification image showing particles ~8µm x 4µm in size.

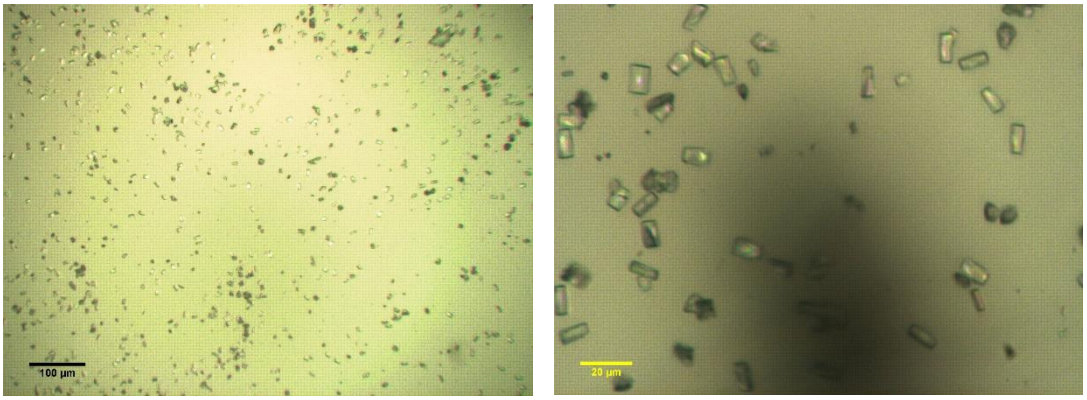

Figure 7. Optical microscopy images showing growth occurring in SI 2.7 solution at ambient temperature with exposure time of ~2 hrs. (a) 2x magnification image; (b) 10x magnification image showing particles ~11µm x 8µm in size.

To get a better understanding of the particle distribution in these images, we divided the image into grids and calculated the approximate number of particles per grid giving us an idea of the number of total particles and thus the particle density. To do that, we calculated the number of particles in grid where more particles appeared as well as in a grid were the particle density was lower. We then found out the average for the particle density and multiplied the data with the number of complete grids in the image. For the incomplete grids, the number was hand counted and added to the data. The data thus collected is displayed in the table given below. The pictures with grids are displayed below as well. The data for SI 2.47 experiment is not considered for this comparison as the exposure time was longer than the experiments involving SI 2.60 and SI 2.70 where the exposure time was ~2hrs.

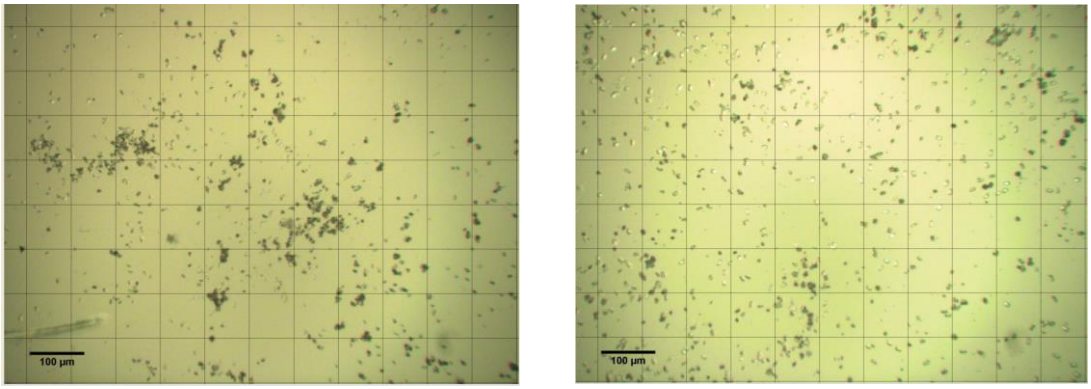

Figure 8. Particle density distribution counting images for varying SI experiment results. (Left) Image for SI 2.6. (Right) Image for SI 2.7.

Table 3. Particle distribution data for experimental set of SI 2.47, 2.6 and 2.7.

SI	Particles per sq um	Total particles
2.6	0.1408	1408
2.7	0.1496	1496

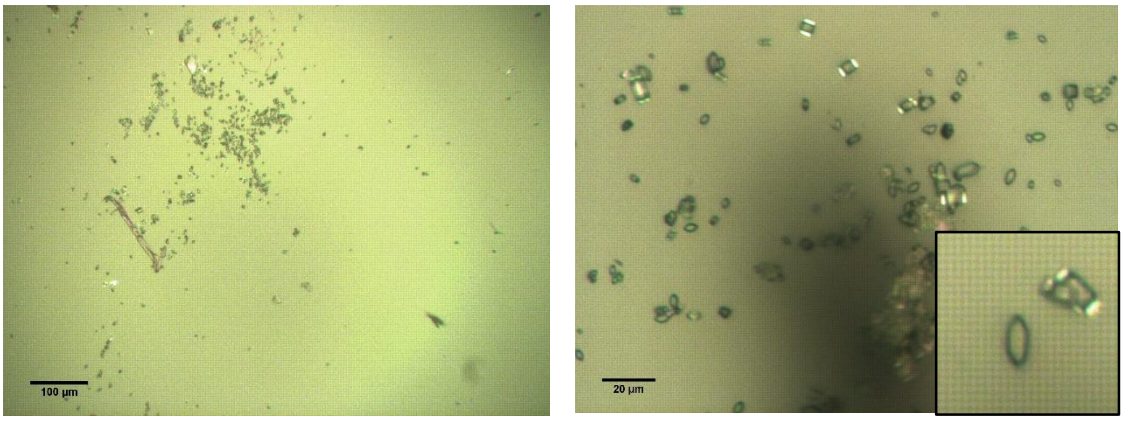

Figure 9. Optical microscopy images showing growth occurring in SI 2.47 solution at 60°C with exposure time of ~2 hrs. (a) 2x magnification image; (b) 10x magnification image showing particles ~5µm x 4µm in size.

To study the effect of temperature on occurrence of nucleation, we conducted two experiments at higher temperature and pressure conditions. The supersaturation for these experiments was maintained at 2.47 and the exposure time was ~2 hrs. The first experiment was conducted at 60°C and 20 psi, the resulting image (Figure 9) showing particles which upon careful inspection were found to display a characteristic hexagonal shape. The second experiment was conducted at 90°C and 60 psi for ~2hrs. Figure 10 shows particles showing a characteristic rhomboidal shape.

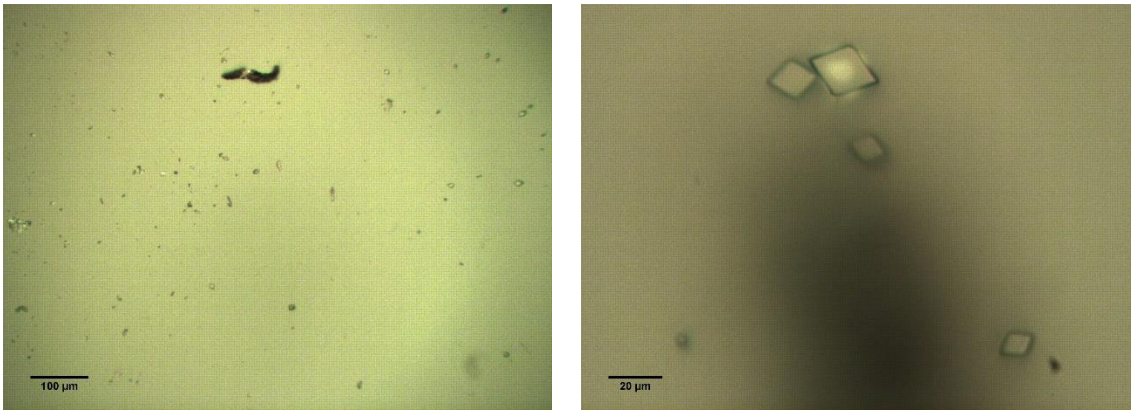

Figure 10. Optical microscopy images showing growth occurring in SI 2.47 solution at 90°C with exposure time of ~2 hrs. (a) 2x magnification image; (b) 10x magnification image showing particles ~27µm x 20µm in size.

To create a well-rounded approach to growth and nucleation, we included barium-to-sulfate concentration ratio variations to our changing experimental conditions. This was achieved by keeping other variables such as temperature, pressure and supersaturation constant for ease of comparison.

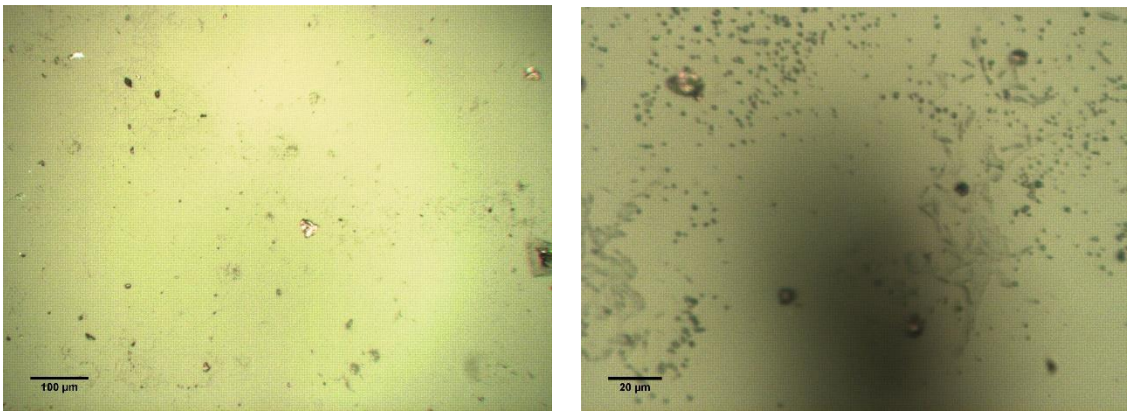

Figure 11. Optical microscopy images showing growth occurring in SI 2.47 solution with a $[Ba^{2+}]$:$[SO_4^{2-}]$ ratio of 10:1. (a) 2x magnification image; (b) 10x magnification image showing particles ~2µm x 2µm in size.

For our first set of ratio experiments, we experimented with solution supersaturation of 2.47 in ambient temperature and 30 psi pressure conditions. The varying $[Ba^{2+}]$: $[SO_4^{2-}]$ ratios included are 10:1, 1:10, 100:1 and 1:100. Figure 11, 12, 13 and 14, respectively, display the results of these experiments.

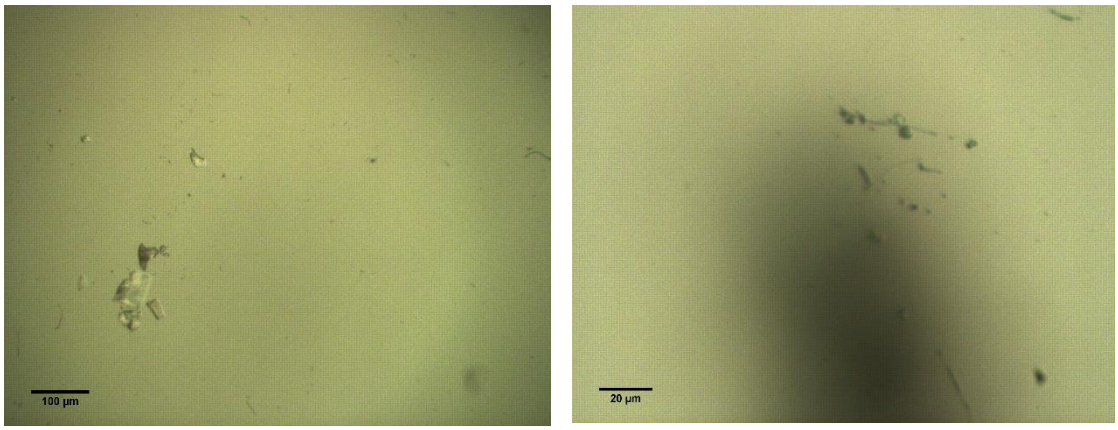

Figure 12. Optical microscopy images showing growth occurring in SI 2.47 solution with a $[Ba^{2+}]:[SO_4^{2-}]$ ratio of 1:10. (a) 2x magnification image; (b) 10x magnification image showing particles ~1µm x 1µm in size.

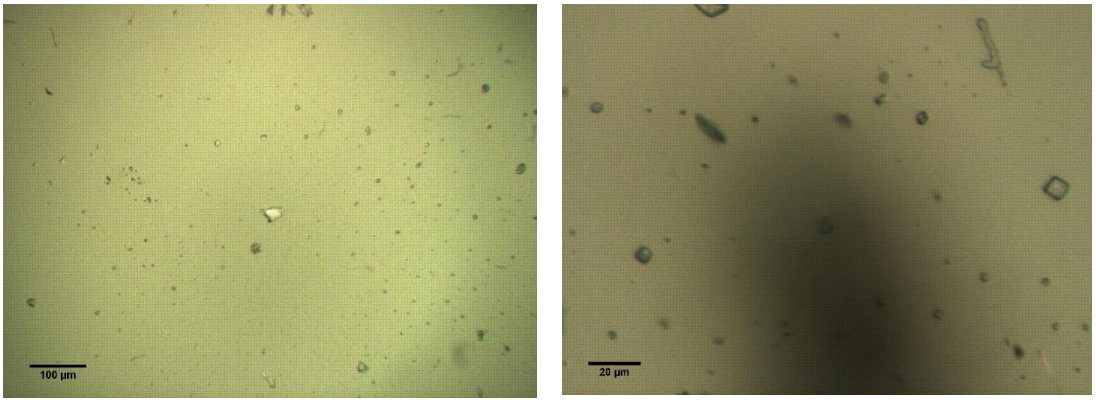

Figure 13. Optical microscopy images showing growth occurring in SI 2.47 solution with a $[Ba^{2+}]:[SO_4^{2-}]$ ratio of 100:1. (a) 2x magnification image; (b) 10x magnification image showing particles ~10µm x 9µm in size

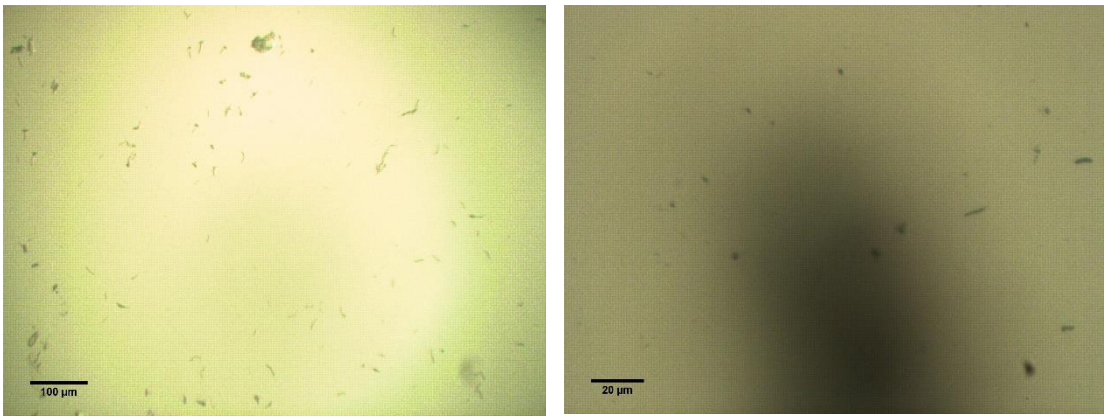

Figure 14. Optical microscopy images showing growth occurring in SI 2.47 solution with a [Ba^{2+}]:[SO_4^{2-}] ratio of 1:100. (a) 2x magnification image; (b) 10x magnification image particles ~1µm x 1µm in size

At a glance, it can be seen that the images with higher [Ba^{2+}] concentrations show more nucleation as compared to those with higher [SO_4^{2-}] concentrations. As a result, the particle sizes are also bigger for the former as compared to the latter. Similarly, the particle sizes are larger for the higher ratio when the two higher [Ba^{2+}] concentration images are compared. Due to their incredibly small sizes, it is difficult to calculate the amount of particles although assessment with the naked eye does give us an idea of the particulate density distribution. It can be ascertained that nucleation is higher in solutions where [Ba^{2+}] ions are available in abundance for their adsorption onto substrates.

For our second set of ratio experiments, we conducted experiments with solution supersaturation of 2.6 at ambient temperature and under 30 psi pressure as with the previous set of experiments, hoping to see more particles nucleating with the increase in SI. This was done so as to allow us to look for trends in nucleation as observed in our previous set of experiments. However, it was observed that the number of particles did not increase as expected instead we saw lower densities of particles for these experiments with the exception of one experimental result.

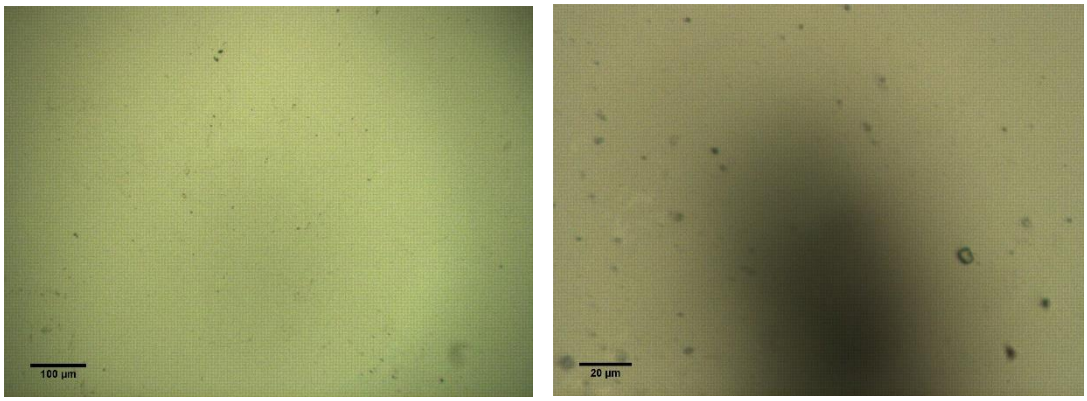

Figure 15.Optical microscopy images showing growth occurring in SI 2.6 solution with a $[Ba^{2+}]:[SO_4^{2-}]$ ratio of 10:1. (a) 2x magnification image; (b) 10x magnification image showing particles ~6µm x 4µm in size

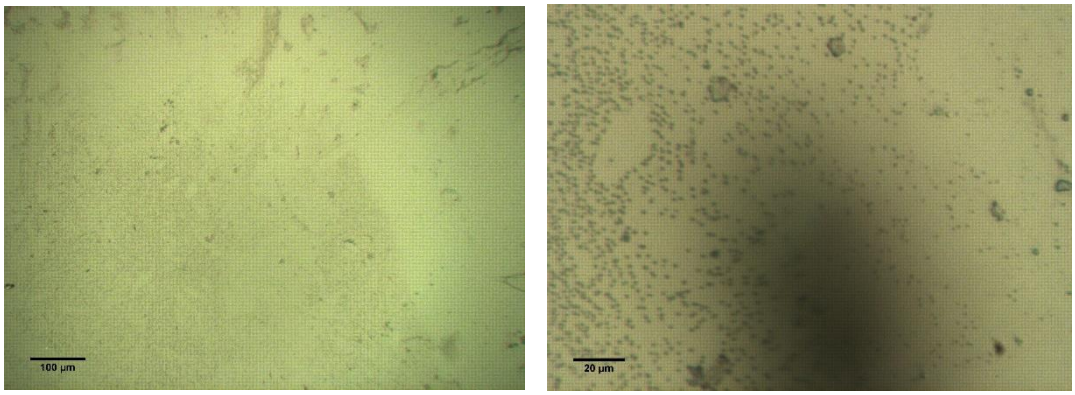

Figure 16. Optical microscopy images showing growth occurring in SI 2.6 solution with a $[Ba^{2+}]:[SO_4^{2-}]$ ratio of 1:10. (a) 2x magnification image; (b) 10x magnification image showing particles ~1.4µm x 1µm in size

In keeping with the observations of the previous set, images with higher [Ba^{2+}] concentrations show more growth and nucleation as compared to those with lower [Ba^{2+}] concentrations with the exception of ratio 1:10 where there is significantly more nucleation occurring as compared to the other ratio experiments in the set. These results would need to be reproduced to deduce whether the observed anomaly in 1:10 ratio experiment appears consistently before drawing any conclusions about the same.

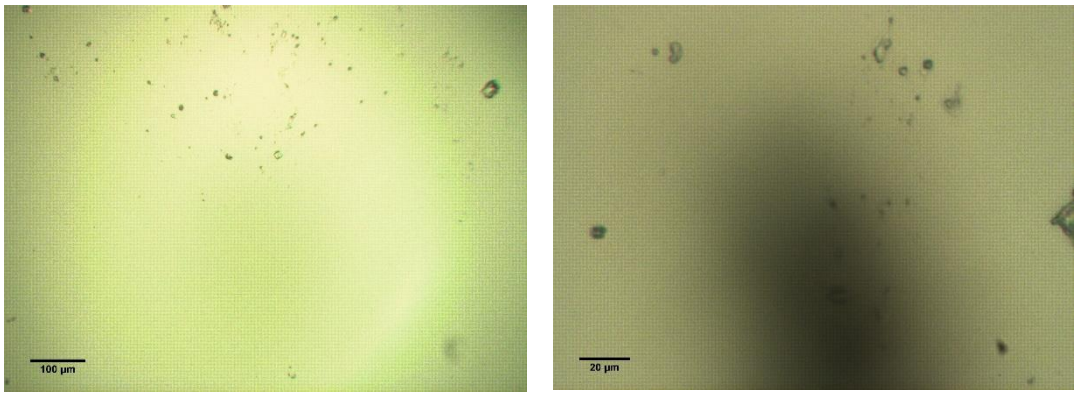

Figure 17. Optical microscopy images showing growth occurring in SI 2.6 solution with a [Ba^{2+}]:[SO_4^{2-}] ratio of 100:1. (a) 2x magnification image; (b) 10x magnification image showing particles ~5µm x 4µm in size

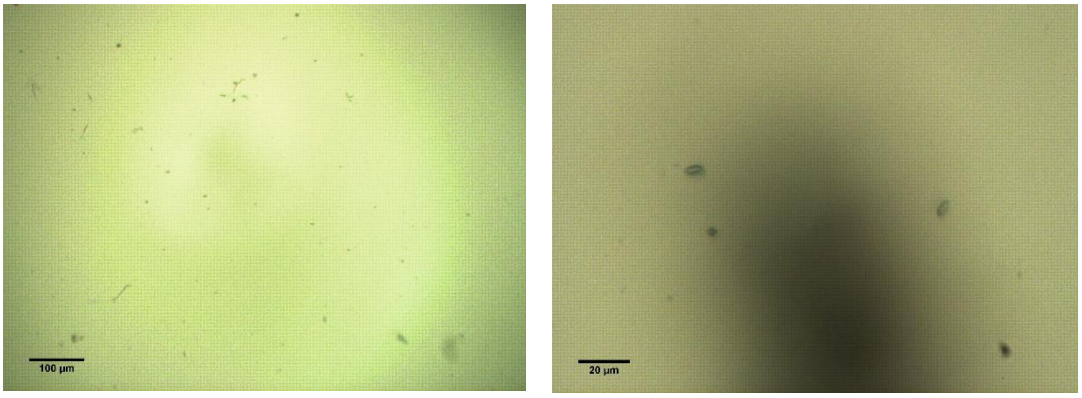

Figure 18. Optical microscopy images showing growth occurring in SI 2.6 solution with a [Ba^{2+}]:[SO_4^{2-}] ratio of 1:100. (a) 2x magnification image; (b) 10x magnification image showing particles ~5µm x 3µm in size

While drawing comparisons between particle sizes of higher concentrations of same ion, it is observed that the particle size is bigger for the higher concentration with the exception of $[Ba^{2+}]$: $[SO_4^{2-}]$ ratio of 100:1 where the particles appear to be only slightly smaller as compared to ratio 10:1.

IV. DISCUSSION

Understanding the mechanisms involved in nucleation and crystal growth of barium sulfate is essential for development of better engineered systems to counteract problematic mineral scaling. By studying heterogeneous nucleation of barite in supersaturated solutions we gained insight into conditions favourable for nucleation.

In investigating growth and nucleation of barite using HAFM, it was observed that the HAFM topographical scans did not show any evidence of nucleation. We speculated the reason behind this observation to be homogeneous nucleation of the supersaturated solution. This could in turn be due to longer solution delivery times leading to an already nucleated solution flowing through the system. As a result, the precipitation of barite on sample glass substrate was not observed because the solution supersaturation was less than the prepared supersaturation. Another reason for the HAFM being unable to detect nucleation could be that the cantilever tip moves the particles along its path of scan. This was later found to not be the case as observing other areas of the substrate confirmed absence of particles.

To counter the issue of homogeneous nucleation of solution and reduce the solution delivery time, we made some changes to our existing solution delivery system. These changes helped reduce the fluid delivery time significantly.

The initial set of experiments conducted with varying solution supersaturations led to the observation that, nucleation and particle density are dependent on supersaturation. When considering nucleation, we know that free energy barrier plays an important role in determining the kinetics of nucleation along with the presence of critical size. When supersaturation is high, the interfacial free energy needed to overcome the energy barrier is

available thus leading to higher nucleation rate in a shorter time of induction. Whereas, when supersaturation is lower, the induction time for nucleation to occur is higher [4].This is as a result of kinetic changes occurring within the solution. Owing to these changes, the free energy barrier gets lowered as the super saturation increases. This reduces the induction time allowing for faster and more nucleation to take place. This claim is supported by our observations of an increasing particle density trend. It should be taken into consideration that the nucleation being high for our SI 2.47 experiment can be attributed to its longer exposure time of 5 hrs 42 mins. Hence, we did not include the data in our comparison in table 3.

When investigating the effect of temperature and solution composition on growth, it was observed that the resulting particles grow in a characteristic shape depending on the conditions. In their studies, Godinho et al [15] talk about the dependence of face specific growth upon solution composition. Their studies suggest that concentration, composition of electrolyte, presence of impurities can act as promoter or inhibitor for specific reactions altering kinetics and crystal shape. They put forth the idea that growth rates along different directions is disproportionately affected by solution composition [13]. The specific growth faces they observed were in solutions containing added electrolytes such as $SrCl_2$ and NaCl. In their studies involving step growth as a function of varying barium to sulfate ratios, Bracco et al [23] observed that as ratios changed, the densities of available sites for nucleation were affected leading to changes in crystal growth. They observed that as the nucleation site density changed, growth along [010] face of the crystal decreased and a more prominent <120> crystal face developed. Drawing collectively upon those ideas, a similar observation can be made for our experimental observations. The change in the solution dynamics as a result of changing experimental conditions and presence of unavoidable impurities plays a role in the

availability of nucleation sites for growth of crystals in characteristic shapes. With our observations, we can confirm that as the temperature increases, the rate at which ions bond will also change leading to slower growth along certain faces (particularly the [010] face). This leads to its disappearance over time as nucleation proceeds. These changes in face specific growth rates can be attributed to bonding and adsorption & desorption of barium and sulfate ions at the nucleation sites [23]. As a result, the particles thus nucleated have a characteristic shape as evident from our results.

Furthermore, Gebauer et al [9] mention the possibility of mesocrystal formation as a step in non-classical nucleation pathway. They put forth the idea of crystallization occurring via amorphous and liquid- precursor pathways suggesting nanoparticles as mesocrystals are capable of orienting themselves and fusing crystallographically ; thus making it difficult to differentiate them from classically formed crystals. This leaves a wide area of crystallization unresolved as what could have been formerly considered classically formed crystals could in fact have been an intermediate phase of crystallization also alternatively recognized as crystal aggregation step in non-classical crystallization. That being said, we cannot eliminate the possibility of presence of an intermediate stage of development in nucleation. The lifetimes and kinetics of these stages are yet to be uncovered.

Early studies describe [Ba^{2+}] dehydration and adsorption onto $BaSO_4$ particles as the controlling step in the growth of $BaSO_4$ in solution[16, 17]. Their findings mention the role of varying lattice ion ratios and supersaturation on nucleation rates. They observed that experiments wherein the [Ba^{2+}]: [SO_4^{2-}] is less than one (excess of sulfate ions) the particle precipitation was found to be lower as opposed to that found in conditions of greater ratio (excess of barium ion). These observations formed the principles behind later experiments

conducted by Dai et al [12]. The outcomes of these experiments claimed that an increase in $[Ba^{2+}]$: $[SO_4^{2-}]$ ratio led to increase in particle size and density [12]. These experiments were conducted upon various organically coated substrates which implies occurrence of chelation. This could in turn be responsible for the high Ba^{2+} adsorption rates thus promoting heterogeneous nucleation in these conditions. This can be attributed to more Ba^{2+} ions being able to bind and adsorb in presence of an ion excess [12]. However, it is also true that an excess of just one ion cannot promote nucleation as rates of nucleation will be affected due to lack of other species.

In keeping with these observations, similar trends were found in our experiments where a higher $[Ba^{2+}]$ showed more nucleation as compared to particles occurring in higher $[SO_4^{2-}]$ conditions.

Given the unstable nature of intermediate phases and precursor particles, it would be of much interest to devise future experiments which allow for periodic analysis of sample as growth is underway. This would allow for tracking of changes occurring in the solution composition as well as in the particles at different stages of nucleation. Not only will this help gain much needed evidence about nucleation but it will also provide in-depth insight into the various steps involved in nucleation. Although given the limitations of optical microscopy and HAFM, it would be beneficial to use instruments such as transmission electron microscopy (TEM), energy dispersive X-rays (EDX), attenuated total reflectance Fourier transform infrared spectroscopy (ATR-FTIR) and grazing-incidence small-angle X-ray scattering (GISAXS) as previously used by Ruiz-Agudo et al[1] and Dai & Stack et al [12] in their studies. This would provide much concrete evidence of existence of non-classical nucleation occurring. To capture that, we will have to devise methods to increase the lifetimes of amorphous phases so as to allow

analysis of the kinetics occurring at those levels. Some distinguishing characteristics of which could be different yet distinct shapes of critical nuclei, induction time for nucleation, kinetics of solution compositions involved, and the distinct physical characteristics of the crystals thus formed.

V. CONCLUSION

While investigating the growth and nucleation of Barite, it was observed that parameters such as supersaturation, temperature and ratio of ion species plays an important role in occurrence of nucleation phenomena. Particle density shows an increasing trend with increase in solution supersaturation. As the supersaturation increases it leads to changes in solution kinetics by lowering the barrier to nucleation. Temperature variations also result in changes in the density of nucleation sites as the solution dynamics change leading to changes in adsorption rates of ions and their bonding. These changes result in characteristically shaped crystal formation (hexagonal and rhomboidal shapes in our case) owing to changes in crystal face specific growth rates. Higher concentration of [Ba^{2+}] ions in solutions is found to promote more growth as compared to [SO_4^{2-}]. As a result, the particle size and density is found to be larger for [Ba^{2+}]: [SO_4^{2-}] ratios greater than 1.

REFERENCES

1. Ruiz-Agudo, C., McDonogh, D., Avaro, J. T., Schupp, D. J., & Gebauer, D. (n.d.). Capturing an amorphous BaSO4 intermediate precursor to barite. In CRYSTENGCOMM (Vol. 22, Issue 8, pp. 1310–1313).
2. Bader, M. S. H. (2007). Sulfate removal technologies for oil fields seawater injection operations. Journal of Petroleum Science and Engineering, 55(1), 93–110.
3. Sorbie, K. S., & Mackay, E. J. (2000). Mixing of injected, connate and aquifer brines in waterflooding and its relevance to oilfield scaling. Journal of Petroleum Science and Engineering, 27(1), 85–106.
4. Vekilov, P. G., & DeYoreo, J. J. (2003a). Principles of Crystal Nucleation and Growth. In Biomineralization. NASA Center for Aerospace Information (CASI).
5. Hohenberg, P. C., & Halperin, B. I. (1977). Theory of dynamic critical phenomena. Reviews of Modern Physics, 49(3), 435–479.
6. Kashchiev D (1999) Nucleation: Basic Theory with Applications. Butterworths, Heinemann, Oxford.
7. Binder, K., & Fratzl, P. (2001). Spinodal Decomposition. In *Phase Transformations in Materials* (pp. 409–480). John Wiley & Sons, Ltd.
8. Kashchiev, D. (2004). Two-dimensional nucleation in crystal growth: thermodynamically consistent description of the nucleation work. *Journal of Crystal Growth*, *267*(3), 685–702.

9. Gebauer, D., & Cölfen, H. (2011). Prenucleation clusters and non-classical nucleation. In *Nano Today* (Vol. 6, Issue 6, pp. 564–584).
10. Higgins, S. R., Eggleston, C. M., Knauss, K. G., & Boro, C. O. (1998). A hydrothermal atomic force microscope for imaging in aqueous solution up to 150 °C. Review of Scientific Instruments, 69(8), 2994–2998.
11. Oshchepkov, M., Popov, K., Ryabova, A., Redchuk, A., Tkachenko, S., Dikareva, J., & Koltinova, E. (2019). Barite crystallization in presence of novel fluorescent-tagged antiscalants. *International Journal of Corrosion and Scale Inhibition*, *8*(4), 998–1021.
12. Dai, C., G, S. A., Ayumi, K., Alejandro, F.-M., Soo, L. S., & Yandi, H. (2016). Heterogeneous Nucleation and Growth of Barium Sulfate at Organic -Water Interfaces: Interplay between Surface Hydrophobicity and Ba2+ Adsorption. *Langmuir*, *32*(21), 5277–5284.
13. Godinho, J. R. A., & Stack, A. G. (2015). Growth kinetics and morphology of barite crystals derived from face-specific growth rates. *Crystal Growth and Design*, *15*(5), 2064–2071.
14. Poonoosamy, J., Klinkenberg, M., Deissmann, G., Brandt, F., Bosbach, D., Mäder, U., & Kosakowski, G. (2020). Effects of solution supersaturation on barite precipitation in porous media and consequences on permeability: Experiments and modelling. *Geochimica et Cosmochimica Acta*, *270*, 43–60.
15. Ruiz-Agudo, Cristina; Ruiz-Agudo, Encarnacion; Putnis, Christine V.; Putnis, Andrew (2015). Crystal Growth & Design, 15(8), 3724-3733.
16. Martin Kucher, Danijel Babic, Matthias Kind (2006). Precipitation of barium sulfate: Experimental investigation about the influence of supersaturation and free lattice ion ratio on particle formation. Chemical Engineering and Processing: Process Intensification, 45(10), 900-907.

17. D.C.Y. Wong, Z. Jaworski, A.W. Nienow(2001). Effect of ion excess on particle size and morphology during barium sulphate precipitation: an experimental study, Chemical Engineering Science, 56(3), 727-734.

18. Blount, C.W. Barite solubilities and thermodynamic quantities up to 300 °C and 1400 bars. Am. Mineral. 1977, 62, 942–957.

19. Deng, N.; Stack, A. G.; Weber, J.; Cao, B.; De Yoreo, J. J.; Hu, Y. Organic-Mineral Interfacial Chemistry Drives Heterogeneous Nucleation of Sr-Rich (Ba x , Sr1-x)SO4 from Undersaturated Solution. *Proc. Natl. Acad. Sci. U. S. A.* **2019**, *116* (27), 13221–13226.

20. C.W. Jones, *Applications of Hydrogen Peroxide and Derivatives*, Royal Society of Chemistry, Cambridge UK, 1999.

21. *The Merck Index*, 13th Ed., Whitehouse Station NJ, Merck & Co. INC., 2001.

22. Division of Research Safety, University of Illinois. https://drs.illinois.edu/Page/SafetyLibrary/PiranhaSolutions (accessed July 30, 2019)

23. Bracco, J. N., Gooijer, Y., & Higgins, S. R. (2016). Hydrothermal atomic force microscopy observations of barite step growth rates as a function of the aqueous barium-to-sulfate ratio. *Geochimica et Cosmochimica Acta*, *183*, 1–13.

APPENDIX A:

Required Stock Volume Calculation:

Stipulate, $[Ba^{2+}] = [SO_4^{2-}] = x^2$

Where, x represents concentration of barium and sulfate respectively.

$K_{sp} = 10^{-9.96}$

$SI \cong \log\frac{\{Ba^{2+}\}\{SO_4^{2-}\}}{K_{sp,barite}}$

For SI = 2.47,

$2.47 \cong \log\frac{(x^2)}{10^{-9.96}}$

$x = 1.8 \times 10^{-4}$

Therefore, volume of solution needed:

$1.8 \times 10^{-4} \times 50 = 10^{-2} \times x$

x = 0.9 mL

Similarly, for SI 2.75, x = 1.242 mL

APPENDIX B

Concentration calculations for solutions to be used in revised system:

Sample calculation for SI 2.47,

M = Molarity; Q = Flow rate

$M_1Q_1 + M_2Q_2 \rightarrow Q_{total}, M_1', M_2'$

Q_1 = 2.5 mL/hr Q_2 = 10mL/hr

$M_1Q_1 = M_2Q_2$

$M_2 = \frac{M_1Q_1}{Q_2}$

$M_1Q_1 = \frac{n_1}{t}$ ….Where, n = volume(mL) and t = time(s)

$M_1' = \frac{M_1Q_1}{Q_1+Q_2}$ .....③ $M_2' = \frac{M_2Q_2}{Q_1+Q_2}$

Substituting M_2 equation in M_2' →

$M_2' = \frac{\frac{M_1Q_1}{Q_2} \cdot Q_2}{Q_1+Q_2}$

∴ $M_2' = \frac{M_1Q_1}{Q_1+Q_2}$

$S.I = \frac{\log[M1' \cdot M2']}{Ksp}$

From Appendix A calculation that S.I required is 2.47 →

$M_1' = M_2' = 1.8 \times 10^{-4}$ M

Thus, $M_1' = \frac{M_1Q_1}{Q_1+Q_2}$

$M_1 = \frac{M1' . (Q_1 + Q_2)}{Q_1} = \frac{1.8 \text{ x } 10^{-4} \text{ x } 12.5}{2.5}$

$\therefore \quad M_1 = 9.8 \text{ x } 10^{-4} \text{ M}$

From equation of $M_2 = \frac{M_1 Q_1}{Q_2} \rightarrow$

$M_2 = \frac{9.8 \text{ x } 10^{-4}}{10}$

$\therefore \quad M_2 = 2.25 \text{ x } 10^{-4} \text{ M}$

Ratio of $M_1 : M_2 = 4:1$

Solution Prepetation :

M_1 volume needed

$9 \text{ x } 10^{-4} \text{ x } 50 = 10^{-2} \text{ x } x$

$\therefore \quad x = 17.775$ ml

M_2 volume needed

$2.25 \text{ x } 10^{-4} \text{ x } 50 = 10^{-2} \text{ x } x$

$\therefore \quad x = 1.125$ ml

SI 2.47; $[Ba^{2+}]$: $[SO_4^{2-}]$ Ratio Calculations

10:1 Ratio

$[Ba^{2+}] = 10x$ and $[SO_4^{2-}] = x$

Ksp = $10^{-9.96}$; S.I = 2.47

S.I = $\frac{\log[Ba^{2+}]\,[SO_4^{2-}]}{Ksp}$

2.47 = $\frac{\log[10x]\,[x]}{10^{-9.96}}$

$10^{2.47} = \frac{[10x]\,[x]}{10^{-9.96}}$

(295.12) (1.0965x10^{-10}) = $[10x]\,[x]$

3.236 x $10^{-8} = 10x^2$

$\therefore$ $\boxed{x = 5.6886 \text{ x } 10^{-5}}$

$\therefore [SO_4^{2-}]$ = 5.6886 x 10^{-5} and $[Ba^{2+}]$ = 5.6886 x 10^{-4}

M = Morality *Q* = Flowrate

$M_1Q_1 + M_2Q_2 = Q_{total}$, $M_1'M_2'$

Q_1= 2 ml/hr M_1=?

Q_2= 10.5 ml/hr M_2=?

$M_1Q_1 = M_2Q_2$

$M_1' = \frac{M_1 \cdot Q_1}{Q_1 + Q_2}$ $M_2' = \frac{M_2 \cdot Q_2}{Q_1 + Q_2}$

$M_1 = \frac{M_1' \cdot (Q_1 + Q_2)}{Q_1}$ $M_2 = \frac{M_2' \cdot (Q_1 + Q_2)}{Q_2}$

$M_1 = \frac{(5.6886 \times 10^{-4}) \cdot (12.5)}{2}$ $M_2 = \frac{(5.6886 \times 10^{-5}) \cdot (12.5)}{10.5}$

∴ $M_1 = 3.555 \times 10^{-3}$ M and $M_2 = 6.772 \times 10^{-4}$ M

10:1 Ratio Volume Calculations

$[Ba^{2+}] = M_1 = 3.555 \times 10^{-3}$ M

$3.555 \times 10^{-3} \times 50 = 10^{-2} \times x$

∴ x = 17.775 ml

$[SO_4^{2-}] = M_2 = 6.772 \times 10^{-5}$ M

$6.772 \times 10^{-5} \times 50 = 10^{-2} \times x$

x = 0.3386 ml

SI 2.47; $[Ba^{2+}]$: $[SO_4^{2-}]$ Ratio Calculations

100:1 Ratio

$[Ba^{2+}] = 100x$ and $[SO_4^{2-}] = x$

Ksp = $10^{-9.96}$; S.I = 2.47

$S.I = \frac{\log[Ba^{2+}][SO_4^{2-}]}{Ksp}$

$2.47 = \frac{\log[100x][x]}{10^{-9.96}}$

$$10^{2.47} = \frac{[100x]\,[x]}{10^{-9.96}}$$

3.236 x 10^{-8} = $100x^2$

∴ $x = 1.798 \text{ x } 10^{-5}$

∴ $[SO_4^{2-}]$ = 1.798 x 10^{-5} and $[Ba^{2+}]$ = 1.798 x 10^{-3}

M = Morality *Q* = Flowrate

$M_1Q_1 + M_2Q_2 = Q_{total}$, $M_1'M_2'$

Q_1= 2 ml/hr M_1=?

Q_2= 10.5 ml/hr M_2=?

$M_1Q_1 = M_2Q_2$

$M_1' = \frac{M_1 \cdot Q_1}{Q_1 + Q_2}$ $M_2' = \frac{M_2 \cdot Q_2}{Q_1 + Q_2}$

$M_1 = \frac{M_1' \cdot (Q_1 + Q_2)}{Q_1}$ $M_2 = \frac{M_2' \cdot (Q_1 + Q_2)}{Q_2}$

$M_1 = \frac{(1.798 \text{ x } 10^{-3}) \cdot (12.5)}{2}$ $M_2 = \frac{(1.798 \text{ x } 10^{-5}) \cdot (12.5)}{10.5}$

∴ M_1= 0.011 M and M_2 = 2.140 x 10^{-5} M

100:1 Ratio Volume Calculations

$[Ba^{2+}] = M_1$ = 0.011 M

0.011 x 50 = 10^{-2} x x

x = 55 ml

∴

$[SO_4^{2-}]$= M_2 = 2.140 x 10^{-5} M

2.140 x 10^{-5} x 50 = 10^{-2} x x

∴ x = 0.107 ml

If stock is more concentrated:

$[Ba^{2+}]$ = M_1 = 0.011 M

0.011 x 50 = 10^{-1} x x

∴ x = 5.5 ml

SI 2.47; $[Ba^{2+}]$: $[SO_4^{2-}]$ Ratio Calculations

1:10 Ratio

$[Ba^{2+}]$ = x and $[SO_4^{2-}]$ = $10x$

Ksp = $10^{-9.96}$; S.I = 2.47

S.I = $\frac{\log[Ba^{2+}]\,[SO_4^{2-}]}{Ksp}$

2.47 = $\frac{\log[x]\,[10x]}{10^{-9.96}}$

$10^{2.47} = \frac{[x]\,[10x]}{10^{-9.96}}$

(3.236 x 10^{-10}) = $[x]\,[10x]$

3.236 x 10^{-9} = x^2

∴ $x = 5.6886 \text{ x } 10^{-5}$

∴ $[SO_4^{2-}] = 5.6886 \text{ x } 10^{-4}$ and $[Ba^{2+}] = 5.6886 \text{ x } 10^{-5}$

M = Morality *Q* = Flowrate

$M_1Q_1 + M_2Q_2 = Q_{total}$, $M_1'M_2'$

Q_1= 2 ml/hr M_1=?

Q_2= 10.5 ml/hr M_2=?

$M_1Q_1 = M_2Q_2$

$M_1' = \frac{M_1 \cdot Q_1}{Q_1 + Q_2}$ $M_2' = \frac{M_2 \cdot Q_2}{Q_1 + Q_2}$

$M_1 = \frac{M_1' \cdot (Q_1 + Q_2)}{Q_1}$ $M_2 = \frac{M_2' \cdot (Q_1 + Q_2)}{Q_2}$

$M_1 = \frac{(5.6886 \text{ x } 10^{-5}) \cdot (12.5)}{2}$ $M_2 = \frac{(5.6886 \text{ x } 10^{-4}) \cdot (12.5)}{10.5}$

∴ $M_1 = 3.555 \text{ x } 10^{-4}$ M and $M_2 = 6.772 \text{ x } 10^{-4}$ M

Volume Calculations

$[Ba^{2+}] = M_1 = 3.555 \text{ x } 10^{-4}$ M

$3.555 \text{ x } 10^{-4} \text{ x } 50 = 10^{-2} \text{ x } x$

∴ x = 1.7775 ml

$[SO_4^{2-}]$= M_2 = 6.772 x 10^{-4} M

6.772 x 10^{-4} x 50 = 10^{-2} x x

∴ x = 3.386 ml

SI 2.47; $[Ba^{2+}]$: $[SO_4^{2-}]$ Ratio Calculations

1:100 Ratio

$[Ba^{2+}]$ = x and $[SO_4^{2-}]$ = $100x$

Ksp = $10^{-9.96}$; S.I = 2.47

S.I = $\frac{\log[Ba^{2+}]\,[SO_4^{2-}]}{Ksp}$

2.47 = $\frac{\log[x]\,[10x]}{10^{-9.96}}$

$10^{2.47} = \frac{[x]\,[100x]}{10^{-9.96}}$

(3.236 x 10^{-8}) = $[x]\,[100x]$

∴ $x = 1.798 \text{ x } 10^{-5}$

$100x$ = 1.798 x 10^{-3}

∴ $[SO_4^{2-}]$ = 1.789 x 10^{-3} and $[Ba^{2+}]$ = 1.798 x 10^{-3}

M = Morality *Q* = Flowrate

$M_1Q_1 + M_2Q_2 = Q_{total}$, $M_1'M_2'$

Q_1= 2 ml/hr M_1=?

Q_2= 10.5 ml/hr M_2=?

$M_1Q_1 = M_2Q_2$

$M_1' = \frac{M_1 \cdot Q_1}{Q_1 + Q_2}$ $M_2' = \frac{M_2 \cdot Q_2}{Q_1 + Q_2}$

$M_1 = \frac{M_1' \cdot (Q_1 + Q_2)}{Q_1}$ $M_2 = \frac{M_2' \cdot (Q_1 + Q_2)}{Q_2}$

$M_1 = \frac{(1.798 \times 10^{-5}) \cdot (12.5)}{2}$ $M_2 = \frac{(1.798 \times 10^{-3}) \cdot (12.5)}{10.5}$

∴ $M_1 = 1.123 \times 10^{-4}$ M and $M_2 = 2.140 \times 10^{-3}$ M

Volume Calculations

$[Ba^{2+}] = M_1 = 1.123 \times 10^{-4}$ M

$1.123 \times 10^{-4} \times 50 = 10^{-2} \times x$

∴ x = 1.7775 ml

$[SO_4^{2-}] = M_2 = 2.140 \times 10^{-3}$ M

$2.140 \times 10^{-3} \times 50 = 10^{-2} \times x$

∴ x = 10.7 ml

S.I 2.60 Ratio Experiment Calculations:

$[Ba^{2+}]$: $[SO_4^{2-}]$ Ratio Calculations

10:1 Ratio

$[Ba^{2+}] = 10x$ and $[SO_4^{2-}] = x$

Ksp = $10^{-9.96}$; S.I = 2.60

S.I = $\frac{\log[Ba^{2+}]\,[SO_4^{2-}]}{Ksp}$

2.60 = $\frac{\log[10x]\,[x]}{10^{-9.96}}$

$10^{2.60} = \frac{[10x]\,[x]}{10^{-9.96}}$

(398.11) (1.0965 x 10^{-10}) = $[10x]\,[x]$

∴ $\boxed{x = 6.6070 \text{ x } 10^{-5}}$

∴ $[SO_4^{2-}]$ = 6.6070 x 10^{-5} and $[Ba^{2+}]$ = 6.6070 x 10^{-4} ---------①

M = Morality *Q* = Flowrate

$M_1Q_1 + M_2Q_2 = Q_{total}$, $M_1'M_2'$

Q_1= 2 ml/hr M_1=?

Q_2= 10.5 ml/hr M_2=?

$M_1 Q_1 = M_2 Q_2$

$M_1' = \frac{M_1 \cdot Q_1}{Q_1 + Q_2}$ $\qquad$ $M_2' = \frac{M_2 \cdot Q_2}{Q_1 + Q_2}$

$M_1 = \frac{M_1' \cdot (Q_1 + Q_2)}{Q_1}$ $\qquad$ $M_2 = \frac{M_2' \cdot (Q_1 + Q_2)}{Q_2}$

$M_1 = \frac{(6.6070 \times 10^{-4}) \cdot (12.5)}{2}$ $\qquad$ $M_2 = \frac{(6.6070 \times 10^{-5}) \cdot (12.5)}{10.5}$

∴ $M_1 = 4.1294 \times 10^{-3}$ M and $M_2 = 7.8655 \times 10^{-5}$ M

Volume Calculations

$[Ba^{2+}] = M_1 = 4.1294 \times 10^{-3}$ M

$4.1294 \times 10^{-3} \times 50 = 10^{-2} \times x$

∴ $x = 0.3932$ ml

$[SO_4^{2-}] = M_2 = 7.8655 \times 10^{-5}$ M

$7.8655 \times 10^{-5} \times 50 = 10^{-2} \times x$

∴ $x = 10.7$ ml

SI 2.60 $[Ba^{2+}]$: $[SO_4^{2-}]$ Ratio Calculations

1:10 Ratio

$[Ba^{2+}] = x$ and $[SO_4^{2-}] = 10x$

From equation ①

$\therefore [SO_4^{2-}] = 6.6070 \times 10^{-4}$ and $[Ba^{2+}] = 6.6070 \times 10^{-5}$

$M_1' = \frac{M_1 \cdot Q_1}{Q_1 + Q_2}$ $M_2' = \frac{M_2 \cdot Q_2}{Q_1 + Q_2}$

$M_1 = \frac{M_1' \cdot (Q_1 + Q_2)}{Q_1}$ $M_2 = \frac{M_2' \cdot (Q_1 + Q_2)}{Q_2}$

$M_1 = \frac{(6.6070 \times 10^{-5}) \cdot (12.5)}{2}$ $M_2 = \frac{(6.6070 \times 10^{-4}) \cdot (12.5)}{10.5}$

$\therefore$ $M_1 = 4.1294 \times 10^{-4}$ M and $M_2 = 7.8655 \times 10^{-4}$ M

Volume Calculations

$[Ba^{2+}] = M_1 = 4.1294 \times 10^{-4}$ M

$4.1294 \times 10^{-4} \times 50 = 10^{-2} \times x$

$\therefore$ $x = 2.0647$ ml

$[SO_4^{2-}] = M_2 = 7.8655 \times 10^{-5}$ M

7.8655 x 10^{-4} x 50 = 10^{-2} x x

∴ x = 3.9327 ml

SI 2.60 Ratio Calculations

$[Ba^{2+}]$: $[SO_4^{2-}]$ = 100:1 Ratio

$[Ba^{2+}] = 100x$ and $[SO_4^{2-}] = x$

Ksp = $10^{-9.96}$; S.I = 2.60

S.I = $\frac{\log[Ba^{2+}]\,[SO_4^{2-}]}{Ksp}$

2.60 = $\frac{\log[100x]\,[x]}{10^{-9.96}}$

$10^{2.60} = \frac{[100x]\,[x]}{10^{-9.96}}$

(398.11) (1.0965 x 10^{-10}) = $[100x]\,[x]$

∴ $x = 2.0893 \times 10^{-5}$

∴ $[SO_4^{2-}]$ = 2.0893 x 10^{-5} and $[Ba^{2+}]$ = 2.0893 x 10^{-3} -------②

$M_1Q_1 + M_2Q_2 = Q_{total}$, $M_1'M_2'$

Q_1= 2 ml/hr M_1=?

Q_2= 10.5 ml/hr M_2=?

$M_1Q_1 = M_2Q_2$

$M_1' = \frac{M_1 \cdot Q_1}{Q_1 + Q_2}$ $M_2' = \frac{M_2 \cdot Q_2}{Q_1 + Q_2}$

$M_1 = \frac{M_1' \cdot (Q_1 + Q_2)}{Q_1}$ $M_2 = \frac{M_2' \cdot (Q_1 + Q_2)}{Q_2}$

$M_1 = \frac{(2.0893 \times 10^{-3}) \cdot (12.5)}{2}$ $M_2 = \frac{(2.0893 \times 10^{-5}) \cdot (12.5)}{10.5}$

∴ M_1 = 0.0131 M and M_2 = 2.4873 x 10^{-5} M

Volume Calculations

$[Ba^{2+}] = M_1$ = 0.0131 M

0.0131 x 50 = 10^{-2} x x

∴ x = 65.5 ml

$[SO_4^{2-}] = M_2$ = 2.4873 x 10^{-5} M

2.4873 x 10^{-5} x 50 = 10^{-2} x x

∴ x = 0.1244 ml

With concentrated stock:

0.0131 x 50 = 10^{-1} x x

x = 6.55 ml

SI 2.60 $[Ba^{2+}]$: $[SO_4^{2-}]$ Ratio Calculations

1:100 Ratio

$[Ba^{2+}] = x$ and $[SO_4^{2-}] = 100x$

From equation ②

$\therefore [SO_4^{2-}] = 2.0893 \times 10^{-3}$ and $[Ba^{2+}] = 2.0893 \times 10^{-5}$

$M_1' = \frac{M_1 \cdot Q_1}{Q_1 + Q_2}$ $M_2' = \frac{M_2 \cdot Q_2}{Q_1 + Q_2}$

$M_1 = \frac{M_1' \cdot (Q_1 + Q_2)}{Q_1}$ $M_2 = \frac{M_2' \cdot (Q_1 + Q_2)}{Q_2}$

$M_1 = \frac{(2.0893 \times 10^{-5}) \cdot (12.5)}{2}$ $M_2 = \frac{(2.0893 \times 10^{-3}) \cdot (12.5)}{10.5}$

$\therefore$ $M_1 = 1.3058 \times 10^{-4}$ M and $M_2 = 2.4873 \times 10^{-3}$ M

Volume Calculations

$[Ba^{2+}] = M_1 = 1.3058 \times 10^{-4}$ M

$1.3058 \times 10^{-4} \times 50 = 10^{-2} \times x$

$\therefore$ $x = 0.6529$ ml

$[SO_4^{2-}] = M_2 = 2.4873 \times 10^{-3}$ M

$2.4873 \times 10^{-3} \times 50 = 10^{-2} \times x$

$x = 12.436$ ml